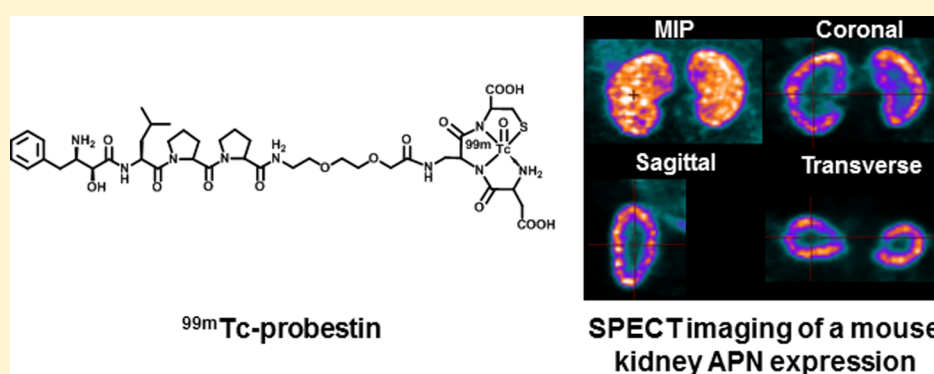


Evaluation of 99m Tc-Probestin SPECT As a Novel Technique for Noninvasive Imaging of Kidney Aminopeptidase N Expression

Gopal Pathuri,^{†,‡} Venkateshwar Madka,[‡] Andria F. Hedrick,[†] Stanley A. Lightfoot,[‡] Vibhudutta Awasthi,^{†,§} Benjamin D. Cowley, Jr.,^{||} Chinthalapally V. Rao,[‡] and Hariprasad Gali*,^{†,§}

[†]Department of Pharmaceutical Sciences, College of Pharmacy, [‡]Center for Cancer Prevention and Drug Development, Hematology/Oncology Section, Department of Medicine, [§]PCS Oklahoma Cancer Center, and ^{||}Nephrology Section, Department of Medicine, College of Medicine, The University of Oklahoma Health Sciences Center, Oklahoma City, Oklahoma 73117, United States



ABSTRACT: Aminopeptidase N (APN; CD13; EC 3.4.11.2) is a zinc-dependent membrane-bound exopeptidase that catalyzes the removal of N-terminal amino acids from peptides. APN is known to be highly expressed on renal cortical proximal tubules. APN expression levels are markedly decreased under the influence of nephrotoxins and in the tumor regions of renal cancers. Thus, molecular imaging of kidney APN expression could provide pathophysiological information about kidneys noninvasively. Probestin is a potent APN inhibitor and binds to APN. Abdominal SPECT imaging was conducted at 1 h postinjection of 99m Tc-probestin in a group of 12 UPII-SV40T transgenic and wild-type mice. UPII-SV40T mice spontaneously develop urothelial carcinoma *in situ* and invasive transitional cell carcinoma (TCC) that invade kidneys. Histopathology and immunohistochemistry analysis were used to confirm the presence of tumor and to evaluate APN expression in kidney. Radioactivity in normal tissue regions of renal cortex was clearly visible in SPECT images, whereas tumor regions of renal cortex displayed significantly lower or no radioactivity uptake. Histopathological analysis of kidney sections showed normal morphology for both renal pelvic and cortical regions in wild-type mice and abnormal morphology in some transgenic mice. Proliferating cell nuclear antigen staining confirmed the presence of tumor in those abnormal regions. Immunohistochemical analysis of kidney sections using anti-CD13 antibody showed significantly lower APN expression in tumor regions compared to normal regions. Results obtained in this study demonstrate the potential use of 99m Tc-probestin SPECT as a novel technique for noninvasive imaging of kidney APN expression.

KEYWORDS: aminopeptidase N, APN, CD13, alanyl peptidase, probestin, renal pathophysiology, renal cancer, SPECT, imaging

INTRODUCTION

Aminopeptidase N (APN; also known as CD13) is a type II membrane zinc-dependent metalloprotease.¹ APN preferentially cleaves neutral amino acids from the N-terminus of peptides. It is expressed in many tissues, being most abundant in the enterocytes of the small intestine and in the epithelium of kidney proximal tubules.² While the exact role of renal APN is not well understood, some studies have suggested that it regulates tubular salt handling, influences blood pressure, and plays a pathogenic role in hypertension.³ APN converts angiotensin III to angiotensin IV by cleaving N-terminal arginine.⁴ Previously APN was proposed as a urinary biomarker of renal disease since it is present at low levels in normal urine.⁵

Its presence is believed to be due to the turnover of the renal proximal tubular epithelium.⁶ Urine APN levels rise markedly under the influence of nephrotoxins affecting the proximal renal tubule or the glomerulus.^{6,7} Thus, we hypothesized that molecular imaging of kidney APN expression noninvasively could provide pathophysiological information about kidneys, which cannot be obtained by serum or urinary biomarkers.

Received: April 18, 2014

Revised: May 23, 2014

Accepted: July 2, 2014

Published: July 2, 2014

In order to test our hypothesis, we selected the UPII-SV40T transgenic mouse model. UPII-SV40T transgenic mice expressing a Simian Virus 40 large T antigen (SV40T) specifically in urothelial cells under the control of the Uroplakin II (UPII) promoter develop bladder carcinoma *in situ* (CIS), as well as invasive and metastatic transitional cell carcinomas (TCCs).⁸ TCCs are also found in renal pelvis and extend to the renal cortex in many of these mice. Kidney APN expression has also been demonstrated to be significantly decreased in renal cancer tissues compared to adjacent normal tissues.⁹

For this study, we used probestin, a known potent APN inhibitor (K_i value of 19 nM),¹⁰ as a targeting reagent. We have previously reported six 99m Tc-labeled probestin conjugates containing a tripeptidic amine–bisamido-thiol (N₃S type) chelator and a polyethylene glycol (PEG) linker.¹¹ These conjugates demonstrated specific APN-binding in both *in vitro* and *in vivo* experiments.¹¹ Among them, [99m Tc]-oxotechnetium(V)-L-aspartyl-L-2,3-diaminopropionyl-L-cysteinylamide-8-amino-3,6-dioxaoctanoic-probestin (herein referred as 99m Tc-probestin, Figure 1) demonstrated the highest kidney

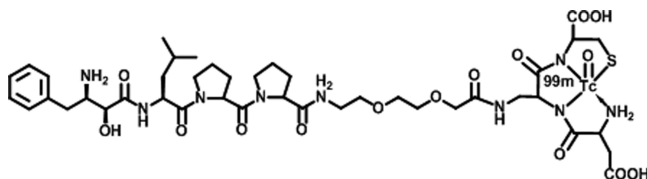


Figure 1. Chemical structure of [99m Tc]oxotechnetium(V)-L-aspartyl-L-2,3-diaminopropionyl-L-cysteinylamide-8-amino-3,6-dioxaoctanoic-probestin (99m Tc-probestin).

uptake. The specific APN targeting of 99m Tc-probestin was confirmed by a blocking biodistribution study in the human fibrosarcoma HT-1080 (these cells are known to express high levels of APN) tumor xenograft-bearing nude mice at 1 h postinjection.^{11c} By coinjection of 100 μ g of probestin with 99m Tc-probestin, over 77% of radioactivity uptake in tumor, kidney, and other APN-expressing tissues was specifically blocked by the excess probestin. Therefore, we selected 99m Tc-probestin as a kidney APN targeting tracer for this study.

MATERIALS AND METHODS

General. Na 99m TcO₄ was obtained from the University of Oklahoma Nuclear Pharmacy. 99m Tc-probestin (Figure 1) was prepared according to our previously reported procedures.^{11a,b} 99m Tc-probestin was obtained in a decay-corrected radiochemical yield of ~60% with radiochemical purity of >98% after HPLC purification. The specific activity of the final product was not determined since the unlabeled probestin conjugate was separated from the radiolabeled product by HPLC. Small animal SPECT imaging was conducted in the OU College of Pharmacy Research Imaging Facility using a two-detector NanoSPECT In Vivo Preclinical Imager (Bioscan, Inc., Washington, DC, USA). All animal studies were conducted in accordance with protocols approved by the University of Oklahoma Health Sciences Center institutional animal care and use committee.

Breeding of UPII-SV40T Transgenic Mice. All mice were bred and genotyped as described earlier.^{8b} In brief, male UPII-SV40T mice were crossed with wild-type females to generate offspring. Transgenic pups were confirmed by tail DNA extraction using the mini-prep kit (Invitrogen) and polymerase

chain reaction (PCR). PCR for the SV40 T gene was done using the primer 5'-CTTTGGAGGCTTCTGGATGCC-ACT-3' (sense) and 5'-GCATGACTCAAAAAACTTAG-CAATTCTG-3' (antisense) and amplifying under the following PCR conditions: denaturation at 95 °C for 5 min, followed by 35 cycles at 95 °C for 1 min, 58 °C for 45 s, and 72 °C for 45 s. The PCR products, when separated on a 2% agarose gel, showed a 550 bp band if the SV40 T gene was present.

Animals were housed in ventilated cages under standardized conditions (21 °C, 60% humidity, 12 h light/12 h dark cycle, 20 air changes per hour) in the University of Oklahoma Health Sciences Center rodent barrier facility. Mice were allowed ad libitum access to standard mouse chow and to automated tap water purified by reverse osmosis.

Small Animal SPECT Imaging. Small animal SPECT imaging was conducted in a total of 12 25–80 week old UPII-SV40T transgenic and wild-type mice (Table 1). Mice were

Table 1. 99m Tc-Probestin Kidney Uptake (% ID/g) at 1 h Postinjection and Histopathology Results of UPII-SV40T Mouse Kidney Sections^a

mouse	genotype	age (wk)	99m Tc-probestin uptake				histopathology			
			LK	RK	LK	RK	LK	RK	LK	RK
1	transgenic	63	36.6	41.0	100	100	5	5		
2	transgenic	57	39.0	48.3	100	100	1	1		
3	transgenic	57	7.6	38.6	100	100	50	5		
4	transgenic	25	63.1	65.4	100	30	5	0		
5	transgenic	25	60.0	65.1	50	100	0	3		
6	transgenic	80	57.1	71.3	0	0	0	0		
7	transgenic	80	65.4	79.3	0	0	0	0		
8	transgenic	50	36.0	38.2	100	100	5	10		
9	transgenic	25	80.1	81.2	100	100	1	0		
10	wild-type	60	56.5	56.6	0	0	0	0		
11	wild-type	80	70.2	87.1	0	0	0	0		
12	wild-type	25	69.6	78.6	0	0	0	0		
99m Tc-probestin uptake										
kidneys										
wild-type mouse kidneys (6 kidneys)										
69.8 ± 12.1										
transgenic mouse kidneys with no damage of renal cortex (7 kidneys)										
68.5 ± 9.2										
transgenic mouse kidneys with $\geq 1\%$ damage of renal cortex (11 kidneys)										
44.9 ± 19.1										

^aMouse 3 is female, and the other mice are male. LK: left kidney. RK: right kidney.

anesthetized using 2% isoflurane in oxygen at 2 L/min, in a polypropylene induction chamber. When fully anesthetized, a dose of 99m Tc-probestin (18.5 MBq) in 100 μ L of 0.2 M PBS (pH 8) was injected through the tail vein. At 1 h postinjection, mice were anesthetized again and placed on the mouse bed of the NanoSPECT camera. SPECT imaging data was acquired for the abdominal region in a helical scanning mode with 20 projections and an acquisition time of 60 s per projection over the whole body. After imaging was done, all mice were euthanized and kidneys were collected. The radioactivity associated with each kidney was measured on a Cobra II automated gamma counter (Packard Instruments). Kidneys

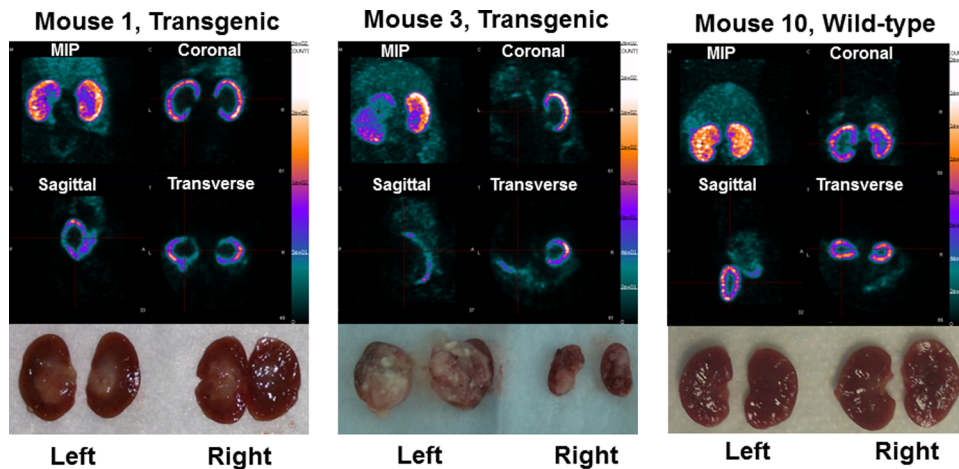


Figure 2. SPECT images obtained at 1 h postinjection of ^{99m}Tc -probestin ($\sim 500 \mu\text{Ci}$) and corresponding kidney photographs. MIP: maximum intensity projection.

were then dissected, photographed, and fixed in 10% neutral-buffered formalin for histopathological evaluation and immunohistochemical analysis.

Raw SPECT imaging data was reconstructed using the software package supplied by the manufacturer. Reconstructed SPECT images were visualized using InVivoScope (Bioscan, Washington, DC) software package.

Tissue Processing and Histopathological Analysis. Formalin-fixed, paraffin-embedded tissues were sectioned (4 μm) and stained with hematoxylin and eosin (H&E). Morphology of each kidney section was evaluated by a pathologist blinded to the experimental group.

Immunohistochemical Analysis. Expression of proliferating cell nuclear antigen (PCNA) and APN (CD13) was evaluated by immunohistochemical analysis. Regions positive for their expression are seen as brown areas in the photographs. Briefly, sections of paraffin-embedded tissues were deparaffinized in xylene, rehydrated through graded ethanol solutions, and washed in phosphate-buffered saline (PBS). Antigen retrieval was carried out by heating the sections in 0.01 mol/L citrate buffer (pH 6.0) for 30 min in a boiling water bath. Endogenous peroxidase activity was quenched by incubation in 3% H_2O_2 in PBS for 5 min. Nonspecific binding sites were blocked using Protein Block for 20 min. Then, sections were incubated overnight at 4 °C with recommended dilutions of monoclonal antibodies, PCNA Antibody (PC10) and CD13 Antibody (C-17) (Santa Cruz Biotechnology), against PCNA (1:800) and APN (1:50) respectively. After several washes with PBS, tissue sections were incubated with appropriate secondary antibodies for 2 h and then exposed to avidin–biotin complex reagent (Invitrogen). After rinsing with PBS, the slides were incubated with chromogen 3,3'-diaminobenzidine for 3 min and then counterstained with hematoxylin. Nonimmune rabbit immunoglobulins were substituted for primary antibodies as negative controls. Specimens were observed using an Olympus IX71 microscope, and digital computer images were recorded with an Olympus DP70 camera.

Statistical Analysis. All results are expressed as the mean \pm SD. To determine the statistical significance of differences between the 2 groups, comparisons were made with the two-tailed Student *t*-test for paired data; a *P*-value of less than 0.05 was considered to be statistically significant.

RESULTS

A group of 12 mice were examined for this study. Genotyping showed that there were nine UPII-SV40T transgenic and three wild-type mice (Table 1). Both the transgenic and wild-type mice were phenotypically similar and did not show overt signs of urothelial tumors.

The SPECT images obtained at 1 h postinjection displayed a high radioactivity uptake in kidneys compared to any other major organ, which is consistent with our previous studies with ^{99m}Tc -probestin.¹¹ Representative SPECT images are shown in Figure 2. As expected, no or minimum uptake of radioactivity was observed in the tumor regions of renal cortex of transgenic mice whereas the entire cortex was visible in wild-type mice (Figure 2). In this group (Table 1), radioactivity uptake in transgenic mouse kidneys with no damage of renal cortex (7 kidneys) was found to be $68.5 \pm 9.2\%$ of injected dose per gram (% ID/g), which was significantly (*P* = 0.002) reduced to $44.9 \pm 19.1\%$ ID/g in transgenic mouse kidneys with at least 1% damage of renal cortex (11 kidneys). The extent of renal cortical damage was quantitatively determined by immunohistochemistry. The radioactivity uptake in wild-type mouse kidneys (6 kidneys) was found to be $69.8 \pm 12.1\%$ ID/g, which matches well with the uptake found in transgenic mouse kidneys with no damage to the renal cortex.

Gross necropsy showed significant tumor growth in kidneys of some transgenic mice (Figure 2). Tumor was observed in one or sometimes both kidneys and mainly occupied renal pelvis but extended into cortex in some mice. Histopathological analysis of kidney sections using H&E staining showed normal morphology for both renal pelvic and renal cortical regions in wild-type mice and abnormal morphology in some transgenic mice. Proliferating cell nuclear antigen staining confirmed the presence of tumor in those abnormal regions (Figure 3, Table 1).

Immunohistochemical analysis of kidney sections using anti-CD13 antibody staining confirmed the reduction of APN expression levels in tumors compared to adjacent normal tissue (Figures 3 and 4).

DISCUSSION

APN plays important roles in angiogenesis, tumor cell invasion, and metastasis.¹² This association of APN with the growth of different human cancers suggested it as a suitable biomarker for

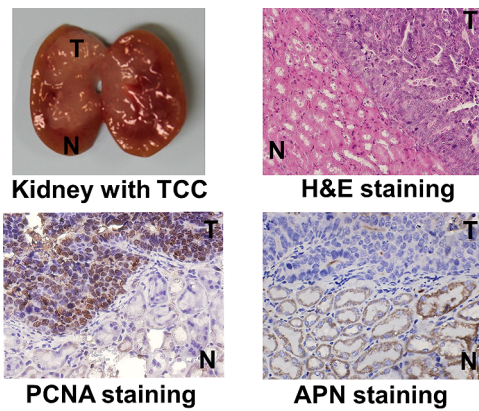


Figure 3. Color images of histopathological and immunohistochemical sections of a UPII-SV40T transgenic mouse kidney. The tumor region (T) is stained positive with both H&E (bluish purple) and PCNA (dark brown) whereas the normal tissue region (N) is stained positive with APN (dark brown).

targeting cancers. Recently, a few SPECT and PET agents based on an APN binding NGR peptide motif have been reported for possible application in imaging APN-positive tumors.¹³ However, these constructs have an asparagine-glycine-arginine (NGR) motif which was found to be rapidly converted to isoaspartate-glycine-arginine (*iso*DGR), an $\alpha_5\beta_3$ integrin binding ligand, by asparagine deamidation.¹⁴ Since the NGR to *iso*DGR transformation may potentially eliminate APN targeting, we chose to examine an alternative APN-binding ligand, probestin, as a vector for targeting APN *in vivo*. For example, NGR peptide-based radiotracers displayed much less (over 10 times) kidney uptake compared to 99m Tc-probestin, even though APN is known to highly express in kidneys.^{11c,13} Although overexpression of APN is generally associated with the presence of tumor, its expression has been shown to be remarkably decreased in the case of renal cancer tissue compared to the surrounding normal tissue in human kidney.⁹ While the precise relation of APN to renal cancer remains unclear, decreased APN expression in renal cancers may be related to decreased zinc levels in renal cancer tissues, since zinc is necessary for the enzymatic activity of APN.^{9a} This differential expression of APN in normal and cancerous kidney tissue could be exploited to obtain useful pathological

information *in vivo* noninvasively. In this regard, to our knowledge this is the first study to investigate the potential use of *in vivo* imaging of kidney APN expression.

In general, an upregulated biomarker is a better choice than a downregulated biomarker for molecular imaging of tumors. However, the main goal of our study was to demonstrate the potential application of imaging APN expression to non-invasively obtain kidney pathophysiological information. We have selected the UPII-SV40T transgenic mouse model because APN-negative invasive and metastatic transitional cell carcinomas are often developed in the renal pelvis in these mice. The progression of these tumors to the renal cortex is thus expected to displace the normal cortical tissue and lead to the absence of the APN expression in the tumor areas. In this study, we correlated histopathological findings of kidney sections with immunohistochemical analysis and 99m Tc-probestin SPECT imaging results of UPII-SV40T transgenic and wild-type mice. Kidney sections of transgenic mice that showed neoplastic abnormalities in renal pelvic and cortical regions by H&E staining also showed strong positive results for PCNA in those regions (Figure 3), while kidney sections from wild-type mice did not exhibit PCNA staining. There was a clear correlation of results obtained by H&E and PCNA staining suggesting that there was significant presence of tumors in some transgenic mouse kidneys. Similarly, immunohistochemical analysis of kidney sections showed significantly higher APN expression in the normal tissue regions of kidneys compared to regions occupied by tumor (Figures 3 and 4). These immunohistochemical results agree well with the previously reported results in renal tissue specimens obtained from clear cell and papillary renal cell carcinoma patients.⁹

As shown in Figure 2, radioactivity in normal tissue regions of renal cortex was clearly visible in SPECT images, whereas tumor regions of renal cortex displayed significantly lower or no radioactivity uptake. As shown in Table 1, radioactivity uptake in transgenic mouse kidneys with no damage of renal cortex is significantly higher (~52%, $P = 0.002$) than in transgenic mouse kidneys with at least 1% damage of renal cortex. At the same time, radioactivity uptake in wild-type mouse kidneys matches well with the uptake found in transgenic mouse kidneys with no damage of renal cortex. The intestinal uptake of radioactivity was visible in the SPECT images (Figure 2) in the abdominal region, especially, in the maximum intensity

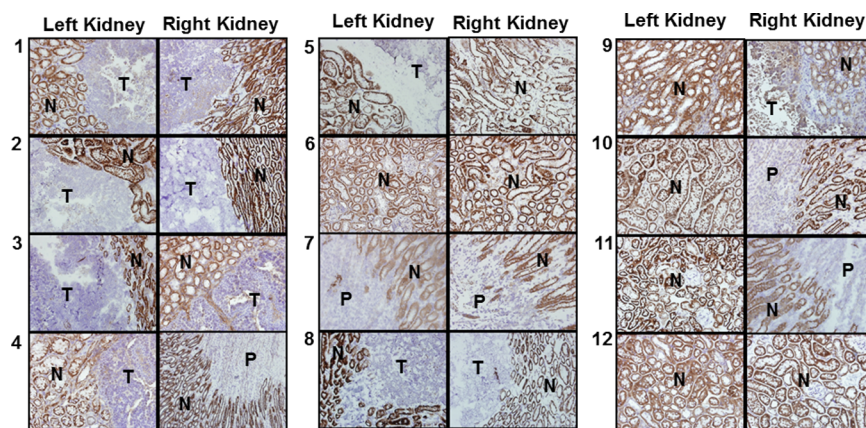


Figure 4. Color images of immunohistochemical sections of all mouse kidneys stained for APN expression. All images were taken in 40 \times magnification. Positive regions are as seen dark brown, and negative regions are represented by light brown to blue staining. N: normal. T: tumor. P: pelvis.

projection images. The relative intensity of this background is low because the uptake ratio of kidney/intestine is >7 (based on biodistribution data from our previously reported studies). The APN-specific uptake of ^{99m}Tc -probestin in intestine was confirmed in our previously reported blocking (with coinjection of 100 μg of probestin with ^{99m}Tc -probestin) biodistribution study in the HT-1080 tumor-bearing mice at 1 h post-injection.^{11b} We observed a blocking of $>77\%$ uptake in intestine as well as other APN-expressing tissues.

In the present study, the SPECT imaging results correlated well with the variation of APN expression levels as indicated by immunohistochemical analysis using anti-CD13 antibody. Thus, absence or markedly reduced radioactivity uptake in tumor regions of renal cortex in this case is attributed to decreased APN expression in those regions based on our immunohistochemical results. However, it is important to note that the decreased uptake of radioactivity could be the result of other unrelated factors such as changes in blood perfusion in tumor regions. In that case additional studies using functional CT or MRI to evaluate the blood perfusion in tumor regions could rule out the false positive results obtained by SPECT imaging of kidney APN expression.¹⁵ In general, the renal function (glomerular filtration rate, GFR) is known to decline steadily with aging after a certain age (in humans beginning at age 30–40 years). In addition to glomerular filtration, renal clearance also occurs via tubular secretion which is preserved even with aging. In the case of APN, since it is expressed in the epithelium of renal proximal tubules, any damage to the glomeruli with aging can affect renal function, but since whole nephron is preserved, blood would still flow through the peritubular capillaries and the tracer present in blood would have access to bind APN. Thus, we think renal function or aging alone may not affect the tracer binding to the APN. This speculation is supported by our observation that, regardless of age (25 to 80 week), all wild-type mice showed very similar kidney uptake of tracer (Table 1).

CONCLUSIONS

Results obtained in this study demonstrate the potential use of ^{99m}Tc -probestin SPECT as a novel technique for noninvasive imaging of kidney APN expression.

AUTHOR INFORMATION

Corresponding Author

*The University of Oklahoma College of Pharmacy, 1110 N. Stonewall Avenue, Room 301, Oklahoma City, OK 73117 United States. E-mail: hgali@ouhsc.edu. Phone: (405) 271-6593 ext 47877. Fax: (405) 271-7505.

Notes

The authors declare no competing financial interest.

ACKNOWLEDGMENTS

This work was funded by an OU College of Pharmacy Startup Grant and NIH NCI-N01CN-53300. We acknowledge funding from NIH Grant S10RR025652 for the NanoSPECT system. We acknowledge the OU Nuclear Pharmacy staff for providing Tc-99m.

REFERENCES

- (1) Sjostrom, H.; Noren, O.; Olsen, J. *Adv. Exp. Med. Biol.* **2000**, *477*, 25–34.
- (2) (a) Kenny, A. J.; Maroux, S. *Physiol. Rev.* **1982**, *62* (1), 91–128. (b) Jardinaud, F.; Banisadr, G.; Noble, F.; Melik-Parsadaniantz, S.; Chen, H.; Dugave, C.; Laplace, H.; Rostene, W.; Fournie-Zaluski, M. C.; Roques, B. P.; Popovici, T. *Biochimie* **2004**, *86* (2), 105–113. (c) Stange, T.; Kettmann, U.; Holzhausen, H. J. *Eur. J. Histochem.* **2000**, *44* (2), 157–164.
- (3) (a) Danziger, R. S. *Heart Failure Rev.* **2008**, *13* (3), 293–298. (b) Kotlo, K.; Shukla, S.; Tawar, U.; Skidgel, R. A.; Danziger, R. S. *Am. J. Physiol.* **2007**, *293* (4), F1047–F1053. (c) Kotlo, K.; Hughes, D. E.; Herrera, V. L.; Ruiz-Opazo, N.; Costa, R. H.; Robey, R. B.; Danziger, R. S. *Hypertension* **2007**, *49* (3), 467–472. (d) Farjah, M.; Washington, T. L.; Roxas, B. P.; Geenen, D. L.; Danziger, R. S. *Hypertension* **2004**, *43* (2), 282–285.
- (4) Ardaillou, R.; Chansel, D. *Kidney Int.* **1997**, *52* (6), 1458–1468.
- (5) (a) Peters, J. E.; Mampel, E.; Schneider, I.; Burchardt, U.; Fukala, E.; Ahrens, I.; Haschen, R. J. *Clin. Chim. Acta* **1972**, *37*, 213–224. (b) Mattenheimer, H.; Frolik, W.; Grotsch, H.; Maruhn, D.; Simane, Z. *J. Clin. Chem. Clin. Biochem.* **1988**, *26* (10), 635–644. (c) Holdt, B.; Peters, E.; Nagel, H. R.; Steiner, M. *Clin. Chem. Lab. Med.* **2008**, *46* (4), 537–540. (d) Quesada, A.; Vargas, F.; Montoro-Molina, S.; O’Valle, F.; Rodriguez-Martinez, M. D.; Osuna, A.; Prieto, I.; Ramirez, M.; Wangenstein, R. *PLoS One* **2012**, *7* (7), e40402. DOI: 10.1371/journal.pone.0040402.
- (6) (a) Price, R. G. *Toxicology* **1982**, *23* (2–3), 99–134. (b) Raab, W. P. *Clin. Chem.* **1972**, *18* (1), 5–25.
- (7) Scheler, F.; Bergmann, H. *Proc. Eur. Dial. Transplant Assoc.* **1964**, *1*, 129–131.
- (8) (a) Zhang, Z. T.; Pak, J.; Shapiro, E.; Sun, T. T.; Wu, X. R. *Cancer Res.* **1999**, *59* (14), 3512–3517. (b) Madka, V.; Zhang, Y.; Li, Q.; Mohammed, A.; Sindhwan, P.; Lightfoot, S.; Wu, X. R.; Kopelovich, L.; Rao, C. V. *Neoplasia* **2013**, *15* (8), 966–974.
- (9) (a) Ishii, K.; Usui, S.; Yamamoto, H.; Sugimura, Y.; Tatematsu, M.; Hirano, K. *J. Biochem.* **2001**, *129* (2), 253–258. (b) Blanco, L.; Perez, I.; Sanz, B.; Gil, J.; Lopez, J. I.; Ugalde, A.; Varona, A.; Larrinaga, G. *Anticancer Res.* **2010**, *30* (4), 1137–1141.
- (10) Aoyagi, T.; Yoshida, S.; Nakamura, Y.; Shigihara, Y.; Hamada, M.; Takeuchi, T. *J. Antibiot. (Tokyo)* **1990**, *43* (2), 143–148.
- (11) (a) Pathuri, G.; Hedrick, A. F.; Disch, B. C.; Doan, J. T.; Ihnat, M. A.; Awasthi, V.; Gali, H. *Bioconjugate Chem.* **2012**, *23* (1), 115–124. (b) Pathuri, G.; Hedrick, A. F.; Disch, B. C.; Ihnat, M. A.; Awasthi, V.; Gali, H. *Bioorg. Med. Chem. Lett.* **2012**, *22* (14), 4567–4570. (c) Pathuri, G.; Hedrick, A. F.; Awasthi, V.; Ihnat, M. A.; Gali, H. *Bioorg. Med. Chem. Lett.* **2013**, *23* (18), 5049–5052.
- (12) (a) Bhagwat, S. V.; Lahdenranta, J.; Giordano, R.; Arap, W.; Pasqualini, R.; Shapiro, L. H. *Blood* **2001**, *97* (3), 652–659. (b) Bhagwat, S. V.; Petrovic, N.; Okamoto, Y.; Shapiro, L. H. *Blood* **2003**, *101* (5), 1818–1826. (c) Guzman-Rojas, L.; Rangel, R.; Salameh, A.; Edwards, J. K.; Dondossola, E.; Kim, Y. G.; Saghatelian, A.; Giordano, R. J.; Kolonin, M. G.; Staquicini, F. I.; Koivunen, E.; Sidman, R. L.; Arap, W.; Pasqualini, R. *Proc. Natl. Acad. Sci. U.S.A.* **2012**, *109* (5), 1637–1642. (d) Fukasawa, K.; Fujii, H.; Saitoh, Y.; Koizumi, K.; Aozuka, Y.; Sekine, K.; Yamada, M.; Saiki, I.; Nishikawa, K. *Cancer Lett.* **2006**, *243* (1), 135–143. (e) Hashida, H.; Takabayashi, A.; Kanai, M.; Adachi, M.; Kondo, K.; Kohno, N.; Yamaoka, Y.; Miyake, M. *Gastroenterology* **2002**, *122* (2), 376–386. (f) Ishii, K.; Usui, S.; Sugimura, Y.; Yoshida, S.; Hioki, T.; Tatematsu, M.; Yamamoto, H.; Hirano, K. *Int. J. Cancer* **2001**, *92* (1), 49–54. (g) Fujii, H.; Nakajima, M.; Saiki, I.; Yoneda, J.; Azuma, I.; Tsuruo, T. *Clin. Exp. Metastasis* **1995**, *13* (5), 337–344. (h) Saiki, I.; Yoneda, J.; Azuma, I.; Fujii, H.; Abe, F.; Nakajima, M.; Tsuruo, T. *Int. J. Cancer* **1993**, *54* (1), 137–143. (i) Petrovic, N.; Schacke, W.; Shapiro, L. H. CD13/Aminopeptidase N in Tumor Growth and Angiogenesis Aminopeptidases in Biology and Disease. In *Aminopeptidases in Biology and Disease*; Hooper, N. M., Lendeckel, U., Eds.; Kluwer Academic/Plenum Publishers: New York, 2004; Vol. 2, pp 179–200. (j) Pasqualini, R.; Koivunen, E.; Kain, R.; Lahdenranta, J.; Sakamoto, M.; Stryhn, A.; Ashmun, R. A.; Shapiro, L. H.; Arap, W.; Ruoslahti, E. *Cancer Res.* **2000**, *60* (3), 722–727.

(13) (a) Zhang, J.; Lu, X.; Wan, N.; Hua, Z.; Wang, Z.; Huang, H.; Yang, M.; Wang, F. *Nucl. Med. Biol.* **2014**, *41* (3), 268–275. (b) Chen, K.; Ma, W.; Li, G.; Wang, J.; Yang, W.; Yap, L. P.; Hughes, L. D.; Park, R.; Conti, P. S. *Mol. Pharmaceutics* **2013**, *10* (1), 417–427. (c) Ma, W.; Kang, F.; Wang, Z.; Yang, W.; Li, G.; Ma, X.; Li, G.; Chen, K.; Zhang, Y.; Wang, J. *Amino Acids* **2013**, *44* (5), 1337–1345.

(14) (a) Curnis, F.; Longhi, R.; Crippa, L.; Cattaneo, A.; Dondossola, E.; Bachi, A.; Corti, A. *J. Biol. Chem.* **2006**, *281* (47), 36466–36476. (b) Curnis, F.; Sacchi, A.; Gasparri, A.; Longhi, R.; Bachi, A.; Doglioni, C.; Bordignon, C.; Traversari, C.; Rizzardi, G.-P.; Corti, A. *Cancer Res.* **2008**, *68* (17), 7073–7082. (c) Spitaleri, A.; Mari, S.; Curnis, F.; Traversari, C.; Longhi, R.; Bordignon, C.; Corti, A.; Rizzardi, G.-P.; Musco, G. *J. Biol. Chem.* **2008**, *283* (28), 19757–19768. (d) Curnis, F.; Cattaneo, A.; Longhi, R.; Sacchi, A.; Gasparri, A. M.; Pastorino, F.; Di Matteo, P.; Traversari, C.; Bachi, A.; Ponzoni, M.; Rizzardi, G.-P.; Corti, A. *J. Biol. Chem.* **2010**, *285*, 9114–9123. (e) Corti, A.; Curnis, F.; Arap, W.; Pasqualini, R. *Blood* **2008**, *112* (7), 2628–2635.

(15) (a) Reiner, C. S.; Roessle, M.; Thiesler, T.; Eberli, D.; Klotz, E.; Frauenfelder, T.; Sulser, T.; Moch, H.; Alkadhi, H. *Invest. Radiol.* **2013**, *48* (4), 183–191. (b) Rosen, M. A.; Schnall, M. D. *Clin. Cancer Res.* **2007**, *13* (2 Part 2), 770s–776s.